Switching and charge-density-wave transport in $NbSe_3$. III. Dynamical instabilities

M. S. Sherwin* and A. Zettl
Department of Physics, University of California, Berkeley, California 94720

R. P. Hall
AT&T Bell Laboratories, Murray Hill, New Jersey 07974-2070

(Received 3 March 1988)

Several unusual dynamical instabilities are found in switching charge-density-wave (CDW) conduction. In samples driven by a dc current, large-amplitude $1/f$ noise and intermittency occur in regions of negative differential resistance. In samples driven by combined dc and low-frequency ac electric fields, we report the first observation of "ac switching noise." The power spectrum of ac switching noise is broadband and has amplitude as much as 10 dB larger than the broadband noise associated with dc sliding CDW conduction. In samples driven by combined dc and high-frequency ac electric fields, a period-doubling route to chaos and related instabilities are observed when the CDW is mode locked. All instabilities are consistent with the phase-slip picture of switching CDW conduction. Mode locking and associated instabilities in switching CDW's are analyzed in terms of the sine circle map, the logistic map, and the theory of noisy precursors.

I. INTRODUCTION

In typical crystals, charge-density waves (CDW's) depin smoothly as the electric field is increased above a threshold field.[1] Successful models of such "nonswitching" CDW conduction treat the amplitude of the CDW as rigid and assign degrees of freedom only to the phase of the CDW. However, some CDW's "switch" abruptly and hysteretically from a low-conductivity pinned state to a high-conductivity depinned state. To successfully model switching CDW conduction, it is necessary to include degrees of freedom for both the amplitude and the phase of the CDW.[2] Switching CDW crystals are thus a unique system in which to study the amplitude dynamics of CDW's. Recent advances in the theory of nonlinear dynamical systems are essential to understanding the highly nonlinear dynamics of switching CDW's.

This paper is the third in a series of experimental[2,3] and theoretical[4] studies on the dynamics of switching crystals of $NbSe_3$. (Each paper contains enough background information on switching CDW's to be read independently.) The first paper in this series[2] describes the response of switching crystals of $NbSe_3$ to dc electric fields. Switching crystals are distinguished from nonswitching crystals by the presence of bulk discontinuities in CDW current[5] and by large amounts of CDW polarization below the switching threshold. A CDW velocity discontinuity implies a local, periodic collapse of the CDW amplitude at a phase-slip center. It is suggested that switching CDW's are pinned by a sparse distribution of "ultrastrong" impurity pinning centers in addition to the usual weak impurities found in nonswitching crystals.

The second paper in this series[3] investigates the response of switching samples of $NbSe_3$ to small-amplitude ac electric fields. Like the ac conductivity of pinned nonswitching CDW's, the ac conductivity of pinned switching CDW's is overdamped. However, in contrast to the ac conductivity of depinned nonswitching CDW's, the ac conductivity of depinned switching CDW's is underdamped.[6] The underdamped nature of the sliding state of switching CDW conduction implies a motion-dependent inertia. It is argued that such pseudoinertia arises naturally in a phase-slip model of switching CDW conduction.

This paper shall explore a series of electronic instabilities that occur only in switching CDW's. The first instabilities occur for dc current-driven switching CDW's and are associated with a region of negative differential resistance (NDR).[7] Large-amplitude $1/f$ noise and intermittency are observed and attributed to the CDW hopping between many metastable sliding states. The second set of instabilities, occupying the major part of this paper, occur in the presence of strong combined ac and dc electric fields.

The response of nonswitching CDW's to combined ac and dc electric fields has in recent years been the subject of many experimental[8-13] and theoretical[14,15] investigations. The external ac electric field interferes with an internal frequency generated by a CDW as it slides through a periodic impurity pinning potential. When the internal frequency locks to the external frequency (mode locking), CDW transport becomes highly coherent and fluctuations are "frozen out."[11] The number of degrees of freedom active in CDW transport is reduced during mode locking.

The response of switching CDW's to combined ac and dc electric fields is more complex. For driving frequencies less than 1 MHz, we report the first observation of a characteristic power spectrum which we call "ac switching noise." The power spectrum of ac switching noise consists of a broadband component which is superimposed on sharp peaks at the drive frequency and its harmonics. The broadband component decreases monotoni-

cally as a function of increasing frequency and is as much as 10 dB larger than the broadband noise associated with sliding CDW conduction in the same sample. ac switching noise occurs when a sample is driven at low frequency repeatedly through the switch in the I-V curve. No comparable instability is observed in nonswitching samples. ac switching noise is attributed to the unpredictability of the depinning process in switching samples.

For driving frequencies greater than 5 MHz, the phase-slip centers[2,5] created during switching CDW conduction appear to synchronize and a qualitatively different regime occurs. The switching CDW mode-locks to the radio-frequency field, and on each mode-locked step a period-doubling route to chaos[16] or related instability is observed. No comparable instabilities are observed in nonswitching CDW's. The period-doubling route to chaos is viewed as the frustrated response of a pseudoinertial switching CDW which is strongly entrained by the radio frequency electric field.

The period-doubling route to chaos is characteristic of systems with few active degrees of freedom.[17] Thus it is reasonable to compare experimental results for mode-locked switching CDW's with the behavior of low-dimensional nonlinear dynamical systems (nonlinear mathematical models with few degrees of freedom). The structure of mode locking and associated instabilities in switching CDW's are in qualitative and quantitative agreement with the predictions of the one-dimensional sine circle map.[18,19] The period-doubling route to chaos in switching CDW's is consistent with the predictions of the logistic map with added noise.[20] Other instabilities are consistent with the theory of "noisy precursors" of dynamical instabilities.[21,22] The agreement between the mode-locking behavior of switching CDW's and the behavior of low-dimensional nonlinear dynamical systems indicates that, as in nonswitching CDW's, the mode-locked state in switching CDW's involves few active degrees of freedom.

The remainder of the paper is organized as follows. Section II describes experimental techniques. Section III describes experimental results. Section IV analyzes the experimental results in terms of the modern theory of nonlinear dynamical systems and the phase-slip model of switching. The paper concludes in Sec. V and future directions for this work are discussed.

II. EXPERIMENTAL TECHNIQUES

Four different samples of undoped $NbSe_3$ were used in this study. The samples are numbered 1–4. The samples were grown by direct reaction of the elements. Samples 1, 3, and 4 were virgin samples which switched without any treatment. Switching was induced in sample 2 by etching in hot, concentrated sulfuric acid.[2]

Samples were mounted in a standard two-probe configuration with silver paint contacts. Samples 1 and 4 were driven in a constant-current configuration. Samples 2 and 3 were driven in a constant-voltage configuration. In the constant-voltage configuration, dc and rf voltage supplies were buffered with a high-speed voltage follower with a bandwidth of 350 MHz and an output impedance of less than 1 Ω. The response of the switching CDW's was determined in current-driven cases by measuring the voltage across the sample, and in voltage-driven cases by measuring the voltage across a small resistor (resistance less than 10% of the sample resistance) in series with the sample. For (voltage-driven) differential conductance measurements, a small, low-frequency (≤ 200 Hz) modulation was added to the dc and rf voltages, and was detected with a lock-in amplifier. Power spectra for frequencies less than 25 kHz were measured with a Hewlett-Packard HP-3582A [fast Fourier transform (FFT)] spectrum analyzer. Power spectra for frequencies greater than 0.5 MHz were measured with a HP-8558B (sweeping filter) spectrum analyzer.

III. EXPERIMENTAL RESULTS

A. Negative differential resistance and intermittency

This section describes electronic instabilities that are observed exclusively in current-driven experiments on switching samples of $NbSe_3$. The phenomena are most dramatic near 40 K, a temperature somewhat higher than that at which hysteretic switching is fully developed.[2,23] At this temperature, when a sample is biased just above threshold, a region of NDR is observed in the dc response. Frequency-domain analysis of the response near the NDR region shows anomalously large $1/f$ noise as well as violent intermittent behavior.[7]

The inset to Fig. 1 shows a direct current-voltage (I-V) plot for a single $NbSe_3$ crystal at $T=40$ K. The position of the first deviation from Ohmic response, i.e., the threshold current I_T, is identified with an arrow. Beginning at I_C, somewhat above I_T, smoothly increasing the current I results in a smooth decrease in the sample voltage. The differential resistance dV/dI is negative in this region. Increasing I further into the nonlinear region results in the differential resistance becoming positive once again. We note the presence of a "step" in the NDR region, in which dV/dI is close to zero over a limited current range.

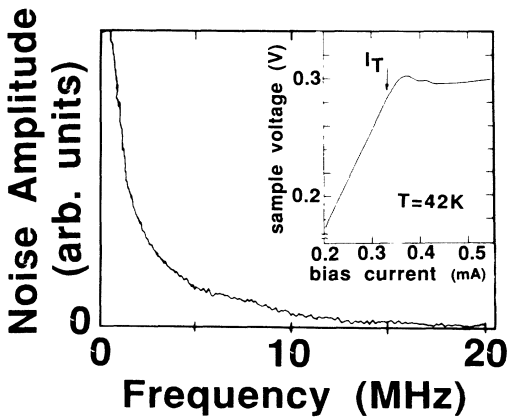

FIG. 1. Power spectrum of the voltage across sample 1 for frequencies less than 20 MHz. The sample was current biased in the negative differential resistance (NDR) region. Inset: I-V curve for sample 1. I_T marks the first deviation from Ohmic behavior. Somewhat above I_T, the region of NDR is visible. A "step" on which $dV/dI \approx 0$ occurs in the NDR region.

Simultaneously with the dc I-V characteristics, the ac voltage response was measured with a spectrum analyzer. The narrow-band and broadband noise generic to CDW conduction starts immediately at I_T. Just before the NDR region, however, a sudden onset of high-level broadband noise occurs, as illustrated in Fig. 1. The power response of the noise signal in Fig. 1 obeys a $1/f$ distribution. At 1 MHz the absolute power level of the noise is approximately 4 orders of magnitude larger than the conventional broadband noise, and approximately 2 orders of magnitude larger than the narrow-band noise, observed immediately before the NDR region. Hence the $1/f$ noise totally dominates the noise usually associated with CDW conduction, which is not observable in Fig. 1. Although the onset of high-level broadband noise corresponds to the beginning of the NDR region, the noise persists even after the current has exceeded the NDR region. However, beyond the NDR region the frequency spectrum becomes distorted and no longer follows a $1/f^a$ behavior.

A second remarkable feature of the spectral response in the NDR region is that of temporal instability. In addition to the large-amplitude $1/f$ noise, power spectra with sharp frequency structure of even larger amplitude appear intermittently. The duration of the additional frequency structure is typically 0.1–0.5 s, and it appears with a frequency ranging from several hertz to approximately 0.1 Hz. The intermittent structure appears only for bias currents in the NDR region. It occurs predominantly on the step $dV/dI=0$ observed within this region. Figure 2 shows the intermittent voltage response in the detection frequency range 0–25 kHz, with the sample current biased to the step in the NDR region shown in the inset to Fig. 1. Figures 2(a)–2(f) are power spectra derived from fast Fourier transforms of time series recorded sequentially and approximately 1 s apart in real time. All other experimental conditions for the plots are identical. The intermittent structure dominates the previously discussed $1/f$ noise: the vertical scale in Fig. 3 is such that the $1/f$ noise discussed previously is largely suppressed. The same dominance of the intermittent structure to the $1/f$ noise was observed in the detection frequency range 1–10 MHz.

The features of NDR and instability described above are temperature dependent. Intermittency and $1/f$ noise were only observed within a few degrees of 40 K. As temperature was raised above 40 K the NDR region became progressively broader, and above approximately 47 K only a smooth decrease in the always-positive differential resistance was observed with increasing current above I_T. As temperature was lowered between 40 and 30 K, the NDR region narrowed and moved closer to I_T. As temperature was lowered below 30 K a gradual transition of the NDR behavior into hysteretic switching was observed (see Ref. 2 for details of the temperature dependence of switching).

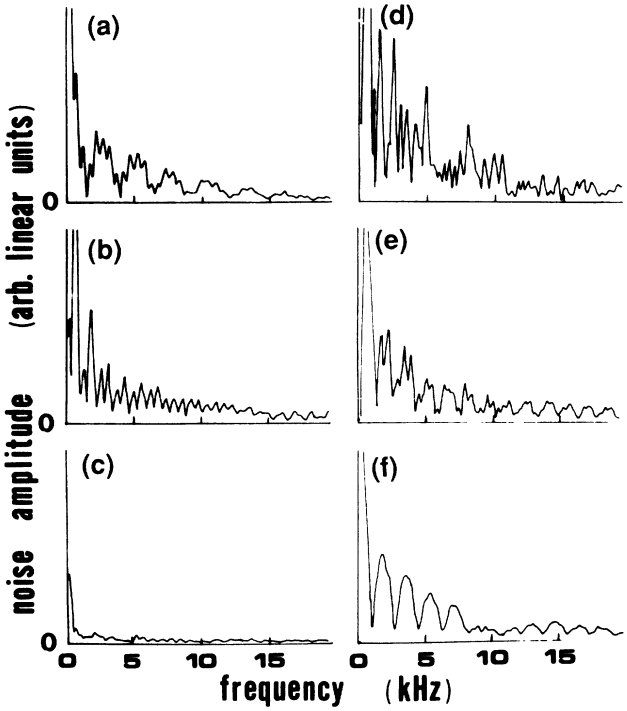

FIG. 2. Power spectra of the voltage across sample 1 for frequencies less than 20 kHz. These power spectra are derived from time series recorded sequentially approximately 1 s apart. For all spectra, sample 1 was held at identical experimental conditions on the $dV/dI\approx 0$ step in the I-V curve.

B. Combined ac and dc electric fields

This section describes the response of switching CDW's to combined ac and dc electric fields. Unless otherwise noted, experiments were performed in a voltage-driven configuration. Section III B 1 describes the ac switching noise which occurs for drive frequencies less than 1 MHz. ac switching noise is attributed to an avalanche depinning process. For rf driving frequencies between 1 and 5 MHz, a crossover takes place to a qualitatively different regime of switching CDW dynamics. Section III B 2 describes the high-frequency regime in which the dynamics are dominated by mode locking and associated period-doubling instabilities. The dynamics in the high-frequency regime are attributed to the phase-slip process.

1. ac switching noise

A characteristic power spectrum which we call "ac switching noise" occurs when dc electric fields are combined with low-frequency (<1 MHz) ac electric fields to drive a sample repeatedly through the switch in the dc I-V curve. (The ac and dc electric fields must satisfy the condition $V_{ac}-V_{dc}<V_C<V_{ac}+V_{dc}$.) The power spectrum defined as ac switching noise consists of a broadband component superimposed on sharp peaks which appear at the driving frequency and its harmonics. The broadband component decreases monotonically as a function of increasing frequency. At a given frequency, the noise power of the ac switching noise is as much as 10 dB larger than the noise power of the conventional broadband noise associated with dc sliding CDW conduction in the same sample. The transition from the quiet state to

the noisy state is abrupt. There are no precursors such as the period-doubling cascade that occurs at higher frequencies in switching $NbSe_3$. ac switching noise is seen for driving frequencies as low as 100 Hz. ac switching noise disappears above the switching onset temperature. Details of the power spectrum of the ac switching noise are shown in Figs. 3 and 4.

Figure 3 compares on a log-log plot the power spectra of the ac switching noise (top trace) and the conventional broadband noise (bottom trace) in the frequency range 25 Hz–25 kHz. The traces are not offset. The top trace was recorded for $V_{dc}=V_C$, $V_{ac}=0.37V_C$, and $f=0.5$ MHz. The noise power in the top trace decreases with increasing frequency. These data are not well fitted by a power law. For frequencies between 25 and 250 Hz, the noise power decreases as roughly $1/f^{0.6}$, while between 2.5 and 25 kHz, the noise power decreases more steeply, roughly as $1/f$. The bottom trace was recorded under identical conditions as the top trace, except that V_{ac} was set to 0 and V_{dc} was increased 10% to $1.1V_C$. The ac switching noise in this frequency range is on the average 5 dB larger than the conventional broadband noise for this set of parameters.

Figure 4 compares on a log-linear plot the ac switching noise and the conventional broadband noise between 0.5 and 2 MHz, frequencies comparable to the rf drive frequency. The experimental conditions are identical to those for the power spectra in Fig. 3. The magnitude of the noise in the rf driven state is roughly 10 dB higher than conventional broadband noise in this frequency range for this set of parameters.

2. *Mode locking in switching CDW's*

This section describes mode locking and associated instabilities which occur for driving frequencies greater than 1 MHz. Section III B 2 a describes the structure of mode locking. Section III B 2 b describes the instabilities that occur during mode locking at temperatures well below the switching transition temperature. Section III B 2 c describes the location of the instabilities in parameter space. Section III B 2 d describes the evolution of the instabilities and of the structure of mode locking as the temperature rises above the switching transition.

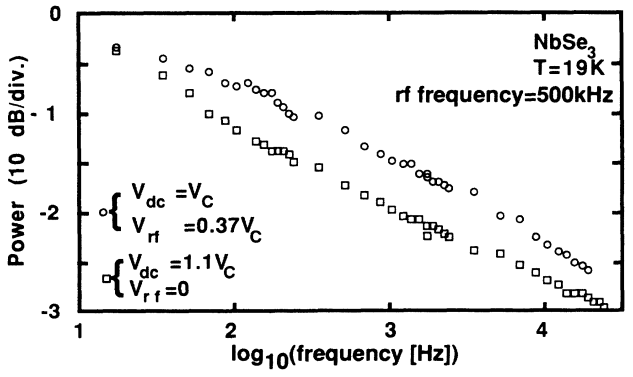

FIG. 3. Power spectrum of the current response in sample 2 for frequencies 25 Hz to 25 kHz: ac switching noise (circles) which is an average of 5 dB larger than the conventional broadband noise (squares). ac switching noise occurs when a sample is driven repeatedly through the switch in the dc I-V curve by combined dc and low-frequency ac electric fields.

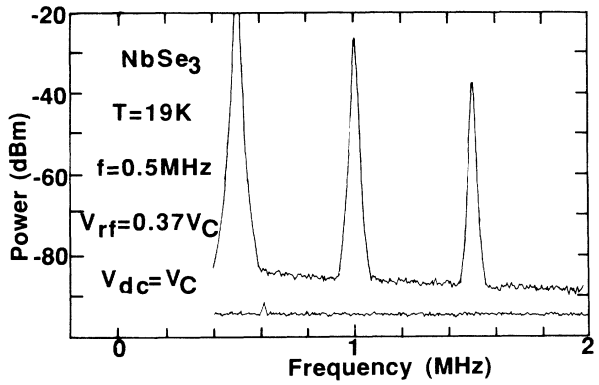

FIG. 4. Power spectrum of the current response in sample 2 for frequencies 0.5–2 MHz: ac switching noise (upper trace) and conventional broadband noise (lower trace). The experimental conditions are identical to those of Fig. 3. The large peaks in the upper trace at 0.5, 1, and 1.5 MHz are at the rf drive frequency and its first and second harmonics. The width of the peaks is instrumental.

a. The structure of mode locking. The structure of mode locking in switching samples is radically different from that of nonswitching samples. In CDW systems driven by combined rf and dc electric fields, mode locking occurs when the "washboard" frequency (generated as the CDW slides through the periodic impurity pinning potential) is a rational multiple of the rf frequency.[8–13] When a CDW is mode locked, the I-V curve shows a step, and the dV/dI curve shows a peak. The structure of mode locking in nonswitching CDW's is illustrated in Ref. 12. For low rf driving amplitudes, the mode-locked steps in nonswitching CDW's are relatively narrow. As the rf amplitude is increased, the width of the mode-locked regions first increases, and then decreases. For any value of rf amplitude, mode-locked peaks in the graph of dV/dI versus I are separated by wide regions in which the CDW is unlocked and dV/dI is low.

Figure 5 shows a series of I-V curves for a switching CDW sample with a clean, strong switch. As the ac amplitude is increased, steps appear in the I-V curve. On each step, the slope of the curve is approximately equal to the slope of the I-V curve below the switching threshold, indicating that the CDW phase velocity is locked to the frequency of the ac drive and the CDW is on a Shapiro step. For instance, the decreasing dc bias curve for $V_{rf}=21$ mV shows that the CDW is *always* mode locked in the region from about 15 to 30 mV of dc bias. When the dc bias reaches the end of a Shapiro step, the system jumps to the next step. The jump is hysteretic—it occurs at different values of the dc bias for sweeps of increasing or decreasing dc bias. For a range of values of rf and dc bias, there are no values of dc bias for which the CDW is not locked. This is even more clear in the lower traces of Fig. 6, in which the (voltage-driven) differential conduc-

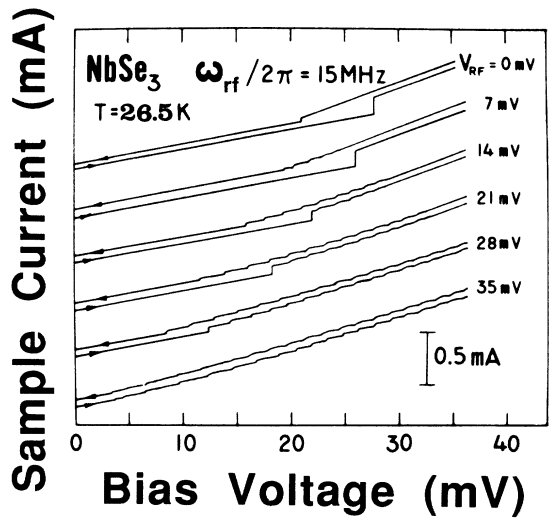

FIG. 5. I-V curves for sample 3 in the switching regime. A rf field induces broad, hysteretic Shapiro steps.

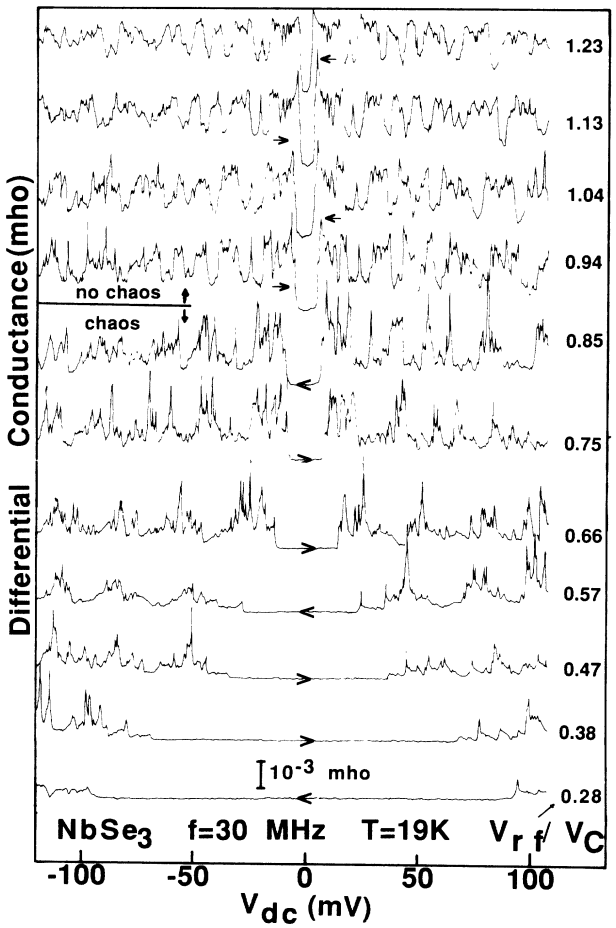

FIG. 6. Differential conductance for sample 2 in the switching regime. Arrows parallel to the differential conductance curves indicate the directions of the voltage sweeps. For low rf electric fields, the differential conductance is always close to the $V_{dc}=0$ value, indicating that most of the sample is mode locked for all values of V_{dc}. Sharp spikes indicate transitions from one mode-locked region to the next. For high rf electric fields, mode-locked regions of low differential conductance are separated by unlocked regions of high differential conductance.

tance is plotted for a different sample in a similar region of parameter space. Mode-locked regions correspond to peaks in differential resistance and hence to troughs in differential conductance. In Fig. 6, sharp spikes in the differential-conductance curves mark the boundaries between Shapiro steps. However, except for the spikes, the differential conductance for moderate dc bias values above the switching threshold field is always close to the differential conductance for a pinned CDW indicating that the system is always at least partially mode locked.[24]

The upper traces of Fig. 6 show that the mode-locked steps take up a smaller fraction of parameter space as rf amplitude or dc bias are increased sufficiently. The Shapiro steps (regions of low differential conductance) are clearly separated by regions in which the CDW is not mode locked and the differential conductance is higher. The structure of mode locking in Fig. 6 at high values of rf amplitude is reminiscent of that seen in nonswitching CDW's at higher temperatures, in which Shapiro steps are always separated by unlocked states. The similarity with higher-temperature data is not a heating effect since the average differential conductance is independent of dc bias for all but the highest rf amplitudes.

b. Instabilities in mode locking for switching CDW's. In mode-locked nonswitching CDW's, velocity fluctuations with frequency much less than the rf frequency are frozen out during mode locking.[11] The broadband noise level at frequencies between harmonics of the rf frequency differs little in mode-locked and unlocked cases.[13] In mode-locked switching CDW's, the power spectrum of the CDW velocity for a constant dc bias may show unusual structure between harmonics of the rf frequency. In (i) of Sec. III B 2 b, we describe a sequence of power spectra which occur as dc bias is swept along n:1 mode-locked steps. This sequence is interpreted as a period-doubling route to chaos. The sequence is nearly periodic in dc bias. In (ii) of Sec. III B 2 b we describe other sequences of power spectra, which are also nearly periodic in dc bias. The latter sequences are explained in Sec. IV in terms of the theory of noisy precursors. In (iii) of Sec. III B 2 b we describe power spectra characteristic of simple mixing between the rf frequency and the narrow-band noise.

(i) Period-doubling route to chaos. The sequence of power spectra identified as a period-doubling route to chaos is shown in Fig. 7(a). The temperature, rf frequency, and rf amplitude are identical in all these spectra. Only the dc bias was changed within a single Shapiro step. The first spectrum shows only the fundamental of the rf drive frequency f, and harmonics due to the nonlinearity of the system. In the second spectrum, peaks appear at $f/2$ and its odd harmonics, indicating the first period-doubling bifurcation in the period-doubling cascade. The third spectrum shows a generally elevated noise level with additional peaks at $f/4$ and its odd harmonics. In the final spectrum broad peaks centered at $f/2$ and odd harmonics are 20 dB above the original noise baseline. We identify the latter spectrum as chaos.

In Fig. 7(b) the dc bias dependence of the power spectrum is mapped out for constant rf amplitude and frequency. Near the end of a given Shapiro step the signal is

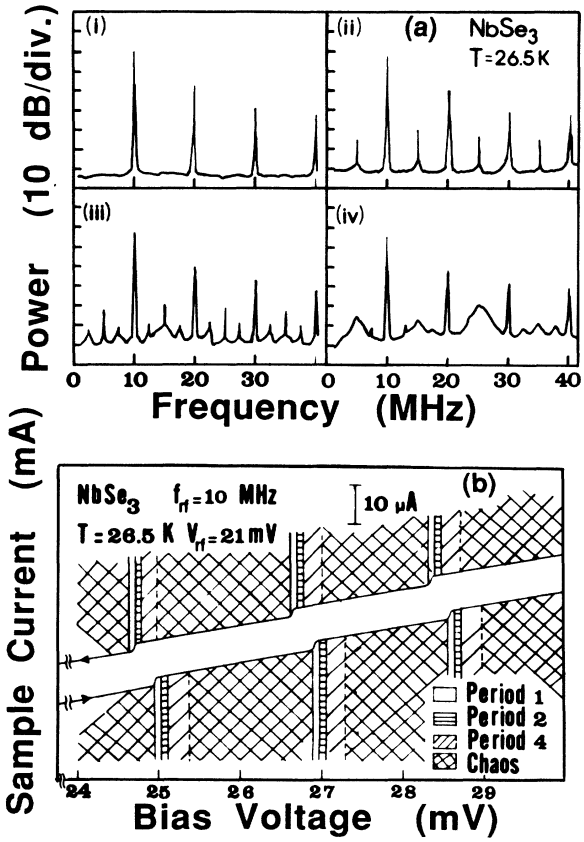

FIG. 7 (a) Power spectra of the current response in the Shapiro-step region of sample 3. External rf drive frequency and amplitude as in (b). (i) $V_{dc}=25$ mV, period 1; (ii) $V_{dc}=25.1$ mV, period 2; (iii) $V_{dc}=25.2$ mV, period 4; (iv) $V_{dc}=25.5$ mV, chaos. (b) Schematic representation of the periodicity of the current response in the Shapiro-step region for sample 3, for forward- and reverse-bias voltage sweeps.

period 1 as in (i) of Fig. 7(a). (Since there is essentially no space between Shapiro steps, and the periodic spectrum occurs over only a small range of dc bias, it was difficult to determine whether this spectrum occurred at the end of one step or the beginning of the next.) The period-1 spectrum was followed by relatively narrow regions of period-2 and period-4 spectra and a broad region of chaotic spectra as shown in (iv) of Fig. 7(a). At the end of a chaotic region, the spectrum again became period 1 and the entire sequence repeated itself on the next Shapiro step. The period-doubling cascade is thus periodic in dc bias over a large range of dc bias. If the dc bias is increased sufficiently, the mode-locking and period-doubling cascades become weaker and eventually evolve into different spectra presented below. The period-doubling route to chaos can also be achieved by varying rf amplitude for fixed rf frequency and dc bias.

Not all switching samples exhibit the period-doubling route to chaos as clearly as the one shown in Fig. 7 (sample 3). For instance, in sample 2, a period-1 spectrum [(i) of Fig. 7(a)] was unattainable in the range of parameters in which period-doubling cascades occurred. At the beginning of a Shapiro step the power spectrum was period 2 as in (ii) of Fig. 7(a) and evolved into chaos as dc bias was increased. As dc was increased further, the system jumped onto the next step where the spectrum was again period 2. Apparently the hysteretic jump always bypassed the region in which the system was period 1.

(ii) Noisy precursors. In addition to the familiar period-doubling route to chaos, a number of more unusual sequences of power spectra also occur in switching $NbSe_3$ crystals. In all spectra shown here the dc bias exceeds the switching threshold, and the rf frequency and amplitude are fixed. One characteristic sequence is shown in Fig. 8. We identify this sequence as an example of the virtual Hopf phenomenon[22] (see Sec. IV). For the lowest dc bias shown (top trace) the spectrum is relatively featureless. As dc bias is increased, broad "bumps" appear symmetrically about $f/2=10$ MHz. These bumps move symmetrically toward 10 MHz, until they become sharp peaks located at approximately $f/3$ and $2f/3$. These peaks broaden again as they move closer to $f/2$ and finally coalesce into a sharp peak at $f/2$. For a finite range of dc bias, the power spectrum does not change. Then the $f/2$ peak suddenly jumps to a lower amplitude and again bumps appear symmetrically about $f/2$. These bumps now move symmetrically away from $f/2$ and eventually disappear. As dc bias is increased further, the identical sequence repeats itself. As in the period-doubling cascade, the sequence of power spectra is nearly periodic in dc bias.

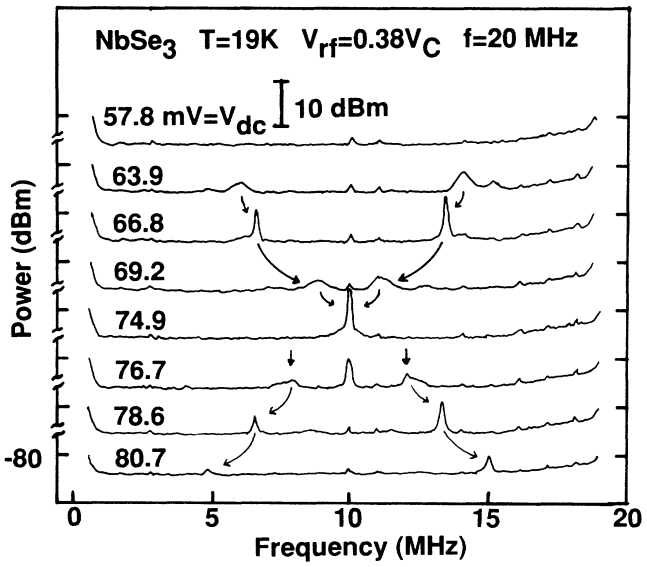

FIG. 8. Sequence of power spectra of the current response of sample 2 for different dc biases at fixed rf amplitude and frequency. The dc bias increases from the top trace to the bottom trace. This sequence is nearly periodic in dc bias. This sequence is identified as an example of the "virtual Hopf phenomenon" [see (iii) of Sec. IV B 2 a]. The power spectra are offset, and each "tic" on the vertical axis is at -80 dBm. The critical field V_C for this sample was 150 mV. The power levels in Figs. 8–10 may be compared with one another as they were recorded for identical amplifier gains and spectrum analyzer bandwidths.

A related sequence of power spectra is shown in Fig. 9. We call this sequence "period 2 with excess noise." In this series the bottom trace represents the smallest value of dc bias. The spectrum for the bottom trace shows only a sharp peak at $f/2=10$ MHz. As dc bias is increased, the amplitude of this peak shrinks continuously until the spectrum changes discontinuously to that shown in the third trace from the bottom, where the peak at $f/2$ has grown by 23 dB and broad symmetric structure appears on the flanks of the $f/2$ peak as well as near the sides of the trace. As the dc bias is increased further, the symmetric structure first smoothly increases and then decreases in magnitude while remaining at the same frequency. Finally, the spectrum changes discontinuously to that of the top trace of Fig. 9, which is virtually identical to the bottom trace. Like the sequence in Fig. 8, this sequence is nearly periodic in dc bias over a broad range of dc bias for constant rf amplitude and frequency.

In the course of sweeping through the large parameter space available in this experiment, spectra such as those depicted in Fig. 10 occurred occasionally. Figure 10(a) shows a power spectrum with a sharp peak at $f/2=5$ MHz and broad peaks symmetrically located at intervals of $f/8$ about the central peak. Figure 10(b) shows a power spectrum with broad peaks at intervals of $f/6$.

(iii) Mixing. There are also V_{rf}-f combinations for which none of the above instabilities occur. In these regions of parameter space, only a weak mixing between the narrow-band noise and the rf field is observed. At a given dc bias, peaks occur at the narrow-band noise frequency f_{NBN}, at the rf frequency f and its harmonics, and at the sum and difference frequencies $nf\pm f_{NBN}$ (n is an integer). As dc bias is swept, the narrow-band noise and sum and difference frequencies move through the spectrum but no behavior obviously different than simple mixing is observed. (For a more extensive description of mixing in nonswitching CDW's, see Ref. 25.)

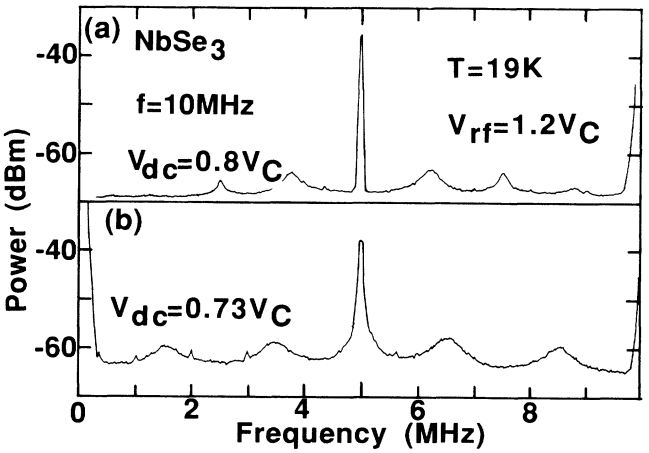

FIG. 10. Power spectra of the current response of sample 2. (a) Period 6, (b) period 8. These power spectra are observed occasionally and do not fit into any clear sequence.

c. Location of the period-doubling and noisy-precursor instabilities in parameter space. This section describes the location in parameter space of the period-doubling and noisy-precursor phenomena. The boundaries of the instabilities described above are convoluted two-dimensional surfaces in a three-dimensional parameter space. We present projections of these surfaces into three different two-dimensional parameter planes.

Figure 11 maps out a region in which period doubling

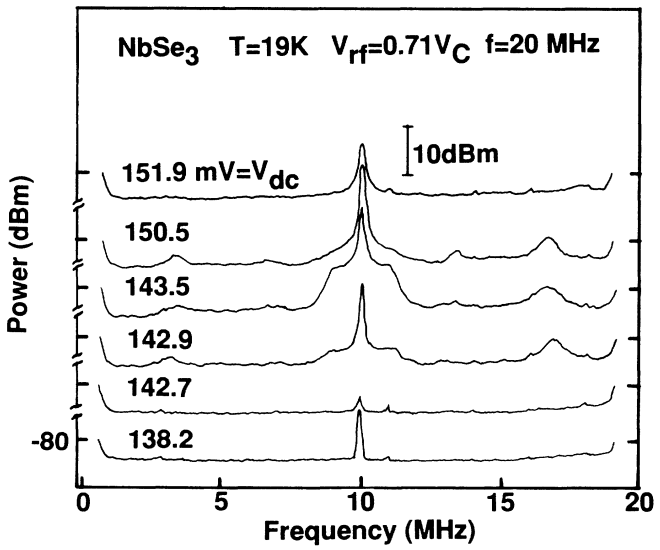

FIG. 9. Sequence of power spectra of the current response of sample 2 for different dc biases at fixed rf amplitude and frequency. The dc bias increases from the bottom trace to the top trace. This sequence, like the sequence in Fig. 8, is nearly periodic in dc bias. We call this sequence "period 2 with excess noise."

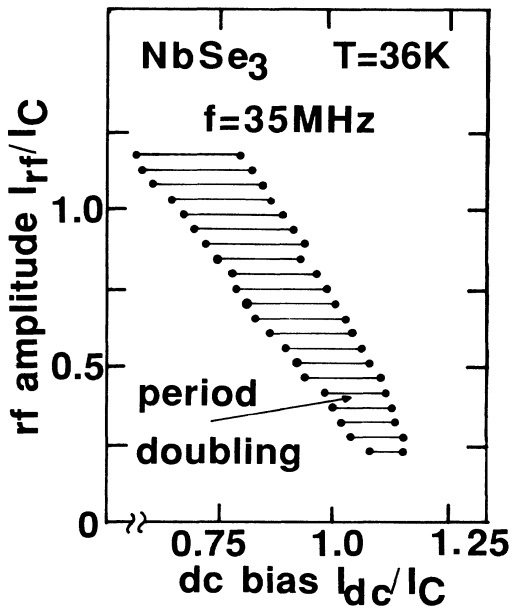

FIG. 11. First period-doubling region in the dc-bias–rf-amplitude plane for sample 4. The figure was constructed by sweeping dc bias forward for rf frequency $f=35$ MHz and various rf amplitudes. The solid circles mark the sudden appearance and disappearance of a strong peak at $f/2$ in the power spectrum.

occurs in the rf-amplitude–dc-bias plane. For these experiments, sample 4 was current driven and the driving frequency was held constant at 35 MHz. The boundaries of this plot were determined by sweeping dc bias at constant rf frequency and amplitude and marking the onset and disappearance of the first period-doubling instability. Because of the relatively high temperature at which these experiments were conducted, the period-doubling cascade never developed into chaos. Figure 11 shows a threshold rf amplitude above which period doubling is possible. As rf amplitude is increased, the dc threshold for the first period-doubling instability decreases. On application of a strong rf electric field, a similar suppression of the CDW depinning threshold occurs in nonswitching samples.[26] A substantial suppression of V_C is also evident in Figs. 5, 6, and 15. The shape of boundary in Fig. 11 is similar for all of the instabilities that are periodic in V_{dc} (i.e., the instabilities described in Sec. III B 2 b). The only qualitative difference is that for some parameter ranges there is an attainable upper V_{rf} threshold above which the instability no longer occurs. The shape of the boundary is also similar for voltage- and current-driven cases.

Figure 12 maps out a region in which period doubling occurs (again, in current-driven experiments on sample 4) in the rf-frequency–dc-bias plane. Figure 12 was constructed in exactly the same number as Fig. 11, except that here the rf amplitude was held constant at $I_{rf}/I_C = 0.71 I_C$. In this case the period-doubling boundary closes on itself, and there are upper and lower limits in dc bias and rf frequency for the first period-doubling instability. As the rf frequency is increased, the lower dc bias threshold for period doubling increases. A similar trend is also seen in the study of ac-dc interference in nonswitching CDW's. As the rf frequency increases for constant rf amplitude, higher narrow-band noise frequencies are required for mode locking to occur and a given $n:m$ mode-locked step moves to higher dc bias values.

The most revealing way in which to map the parameter dependence of the instabilities in mode locking is as a function of rf amplitude and frequency, as is done in Fig. 13. By varying the dc bias at fixed rf amplitude and frequency it is possible to observe a number of different power spectra, as shown in Sec. III B 2 b. We define a ranking of the observed power spectra in order of proximity to the chaotic state: 1, mixing; 2, virtual Hopf (Fig. 8); 3, period 2 [(ii) of Fig. 7(a)]; 4, period 2 with excess noise (Fig. 9); 5, period 4 [(iii) of Fig. 7(a)]; 6, chaos [(iv) of Fig. 7(a)].

In order to generate Fig. 13, rf frequency and amplitude were fixed and dc bias was swept until the power spectrum closest to chaos (as defined in the above ranking scheme) was observed. Consider the system at a point in the frequency-amplitude plane such that the period-doubling route to chaos depicted in Fig. 7 is possible. That point is marked chaotic in Fig. 13, even though

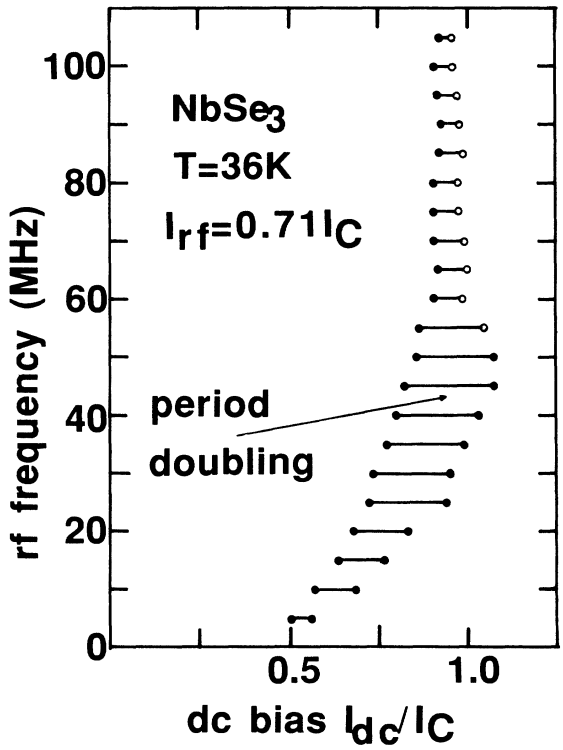

FIG. 12. First period-doubling region in the dc-bias–rf-frequency plane for sample 4. The figure was constructed by sweeping dc bias forward for rf amplitude $I_{rf} = 0.71 I_C$ and various rf frequencies. The solid circles mark the sudden appearance and disappearance of a strong peak at $f/2$ in the power spectrum. For high values of the rf frequency, the $f/2$ peak was not much above the instrumental noise level. The open circles mark the dc biases at which the $f/2$ peak gradually faded into the instrumental noise.

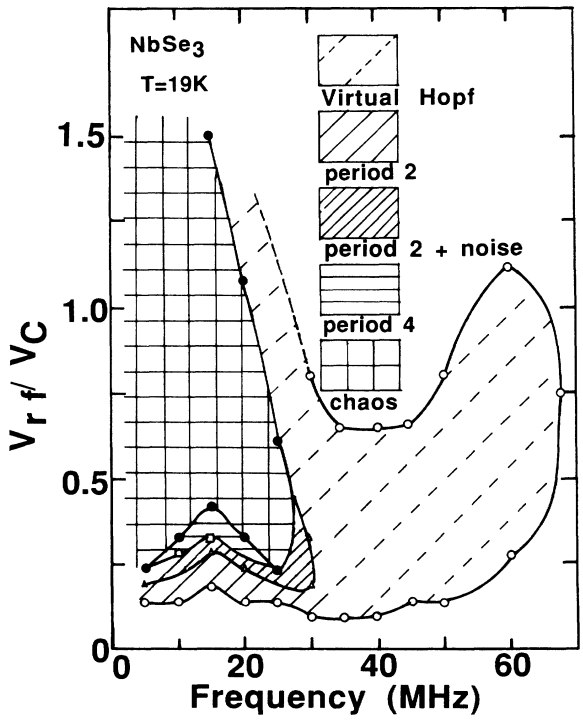

FIG. 13. Location of the instabilities described in Figs. 7–9 in the rf-frequency–rf-amplitude plane for sample 2 for $T < T_{switch}$. The symbols are spaced at 5-MHz intervals and mark the values of rf amplitude at which one type of instability is replaced by another. The lines are guides to the eye.

period-1, -2, and -4 behavior as well as chaos are observed for some values of dc bias. The boundaries drawn in this plot are only approximate, as the instabilities evolve continuously from one type to another. The behavior of switching CDW's at low temperatures may be summarized using Fig. 13 as a guide.

1. For driving frequencies less than 1 MHz, on the left-hand edge of the figure, ac switching noise occurs for $V_{dc}-V_{ac}<V_C<V_{dc}+V_{ac}$. Note the power spectrum we call ac switching noise (Fig. 4) is qualitatively different than the power spectrum we call chaos [(iv) of Fig. 7(a)]. The power spectrum of ac switching noise decreases monotonically between harmonics of the ac driving frequency. The power spectrum of chaos shows broad bumps centered halfway between harmonics of the ac driving frequency.

2. For frequencies between 1 and 5 MHz ac switching noise becomes mixed with a period-doubling route to chaos. ac switching noise is not observed for frequencies greater than 5 MHz.

3. For frequencies between 5 and 30 MHz, a full period-doubling route to chaos may occur for sufficient rf amplitude. The first simple period-doubling instability occurs for rf amplitudes greater than approximately $V_C/10$. As rf amplitude is increased further, period 2 with excess noise (Fig. 9) occurs. For still higher rf amplitude a period-4 instability occurs. Finally, for rf amplitudes greater than $0.4V_C$ the full period-doubling route to chaos is observed. For frequencies between 5 and 15 MHz, a period-doubling route to chaos is observed for the highest rf amplitudes that will not damage the sample. For frequencies between 15 and 30 MHz, increasing the rf amplitude causes the system to exit the region in which the full period-doubling route to chaos occurs. As rf amplitude is increased further, the system first enters a region with only a virtual Hopf sequence. Finally, the system enters a region where only mixing occurs.

4. Above 30 MHz, the period-doubling route to chaos is no longer observed for any rf amplitude. Between 30 and 70 MHz, the most nonlinear behavior is the virtual Hopf behavior sequence of Fig. 8.

5. Above 70 MHz, only mixing is observed.

Figure 13 was constructed for sample 3, but the shape of this plot is similar for different switching CDW samples.

d. Instabilities for $T>T_{switch}$. Just above the switching onset temperature, a number of instabilities disappear. The ac switching noise, which is directly associated with a low-frequency rf field driving the CDW repeatedly through the switch, is no longer present. Neither is a full period-doubling route to chaos observed. However, period-2 and period-4 instabilities, as well as the virtual Hopf (Fig. 8) and period 2 with excess noise (Fig. 9) are still observed. Figure 14 locates these instabilities in rf-frequency–rf-amplitude space. Figure 14 was constructed in the same manner as Fig. 13, but for $T=37$ K instead of $T=19$ K. The boundaries in Fig. 14 are similar to those in Fig. 13, except that certain instabilities no longer appear.

The differential conductance at 37 K for a series of rf amplitudes for rf frequency 50 MHz is shown in Fig. 15. This figure should be compared with Fig. 6. For $V_{rf}=0$, simple CDW depinning is observed. As V_{rf} is increased, troughs develop in the differential conductance, signifying the onset of mode locking. As V_{rf} is increased further, period-doubling instabilities are observed. The mode-locked regions become broad for intermediate values of V_{rf}, filling most of the available range of dc bias at $V_{rf}\approx 0.1V_C$. As V_{rf} is increased further, the mode-locked regions become narrower and period doubling

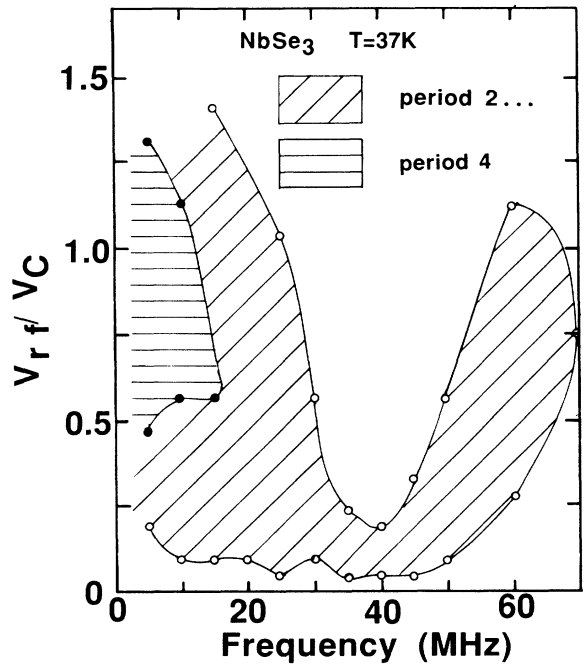

FIG. 14. Location of the instabilities described in Figs. 7–9 in the rf-frequency–rf-amplitude plane for sample 2 for $T>T_{switch}$. The region marked "period 2..." exhibited period 2, period 2 with excess noise, and virtual Hopf behaviors.

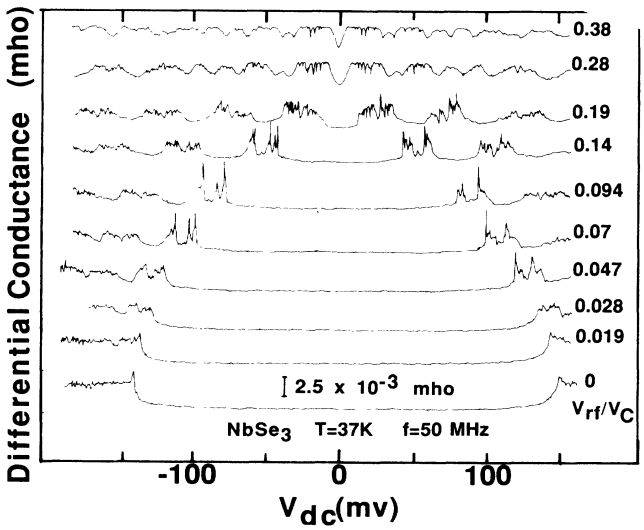

FIG. 15. Differential conductance vs dc bias for sample 2 for $T>T_{switch}$. All voltage sweeps are from left to right.

occurs less frequently. Finally, for $V_{rf} \approx 0.4 V_C$, the differential conductance is high over most of the available range of dc bias, and period doubling occurs not at all. There are two sets of interference troughs in this sample (most clearly visible in the high-V_{rf} data), indicating the presence of two domains with different velocities.

IV. ANALYSIS

The results section of this paper has described a number of unusual instabilities that occur only in switching crystals of $NbSe_3$. In this section these instabilities are analyzed in terms of the phase-slip picture of switching, using simple mathematical models borrowed from the modern theory of nonlinear dynamical systems. A phase-slip model of switching was proposed in the first paper of this series.[2] Anomalies in the ac conductivity of switching CDW's are explained in terms of a phase-slip model in the second paper in this series.[3] Theoretical details of a phase-slip model, and extensive simulations of a differential equation proposed to describe the phase-slip process, are to be found in the fourth paper of this series.[4]

According to the phase-slip picture of switching,[2,4,27] in crystals which show switching at low temperatures, the CDW is pinned by sparsely distributed ultrastrong-pinning centers as well as conventional, weaker impurities. For electric fields below a critical electric field E_C, the CDW becomes heavily polarized, but the ultrastrong-pinning centers prevent it from sliding. The CDW switches and begins to slide only when the polarization energy is sufficiently large to cause the CDW amplitude to collapse at the strongest-pinning centers. When the amplitude collapses, the CDW phase advances by a multiple of 2π, partially relieving the CDW polarization and allowing the CDW amplitude to increase again from zero. However, the CDW polarization rapidly builds up again, causing another amplitude collapse and phase slip. Once the critical field has been exceeded, the CDW advances by periodic slips of the CDW phase. The average pinning force due to the ultrastrong-pinning centers collapses as the electric field is increased above the critical value. Thus, once it depins, the CDW slides with a rapid velocity, comparable to what it would have for the same electric field in the absence of strong-pinning centers.

The instabilities observed in switching samples of $NbSe_3$ can be divided into low- and high-frequency categories. The low-frequency instabilities are the large $1/f$ noise and intermittency associated with negative differential resistance (analyzed in Sec. IV A), and ac switching noise (analyzed in Sec. IV B 1). The low-frequency instabilities are attributed not to the details of the phase-slip process, but to the complex dynamics of many asynchronous phase-slipping domains. The high-frequency instabilities are the period-doubling and related instabilities associated with mode locking (analyzed in Sec. IV B 2). The high-frequency instabilities are attributed to the dynamics of synchronized phase-slipping domains. The mathematical formalism used to describe the instabilities in mode locking is in the sine circle map, which has been used in recent years as a paradigm of mode-locked systems (Sec. IV B 2 a). The physical basis for the observation of period doubling and related instabilities in mode-locked switching CDW's is the motion-dependent inertia associated with the phase-slip process (Sec. IV B 2 b).

A. Negative differential resistance

In this section, negative differential resistance (NDR) and associated instabilities are explained in terms of a phenomenological two-fluid picture. It is shown that NDR may not occur in a voltage-driven CDW. NDR will occur in a current-driven experiment if the CDW current increases sufficiently steeply as a function of applied dc current near threshold. It is suggested that, for dc biases just above threshold, only a fraction of the CDW is depinned and sliding at high velocity. If only a fraction of the CDW is depinned during NDR, the distribution of CDW current within the crystal must be spatially inhomogeneous. The large-amplitude $1/f$ noise and intermittency observed during NDR are attributed to the CDW hopping between the many distributions of CDW current that are accessible for a given dc current bias near threshold.

A CDW crystal can be thought of in terms of a two-fluid model. The current is carried by a channel of normal electrons with a field-independent conductance σ_N in parallel with a CDW channel with a field-dependent conductance σ_{CDW}. Increasing the electric field across a CDW crystal may only cause an increase in CDW current, and hence $d\sigma_{CDW}(V)/dV \geq 0$. This condition is sufficient to show that a voltage-driven CDW may never exhibit NDR. The current through the CDW for a given applied voltage is

$$I = [\sigma_N + \sigma_{CDW}(V)]V \ . \tag{1}$$

The differential conductance [$=1/$(differential resistance)] is

$$\frac{dI}{dV} = [\sigma_N + \sigma_{CDW}(V)] + \frac{d\sigma_{CDW}(V)}{dV} \ , \tag{2}$$

which is always positive. NDR has not been reported in any voltage-driven experiment on $NbSe_3$.

In nonswitching samples, it makes little difference whether a sample is driven by a constant voltage or a constant current. In switching samples, however, the difference may be crucial. For the current-driven case, we begin by assuming that the CDW conductance is a monotonically increasing function only of the applied current I. The voltage V across the CDW crystal is given by

$$V = \frac{I}{\sigma_N + \sigma_{CDW}(I)} \ . \tag{3}$$

The differential resistance is then

$$\frac{dV}{dI} = \frac{1}{[\sigma_N + \sigma_{CDW}(I)]} - \frac{I\sigma'_{CDW}(I)}{[\sigma_N + \sigma_{CDW}(I)]^2} \ , \tag{4}$$

where $\sigma'_{CDW}(I) = d\sigma_{CDW}(I)/dI$. The condition for NDR ($dV/dI < 0$) is

$$\sigma'_{\mathrm{CDW}}(I) > \frac{\sigma_N + \sigma_{\mathrm{CDW}}(I)}{I} . \quad (5)$$

When condition (5) is satisfied, a small increase in current causes a sufficiently large increase in conductivity that the voltage across the sample is a decreasing function of applied current. In nonswitching samples, the CDW conductivity does not increase sufficiently rapidly near threshold to satisfy condition (5). However, condition (5) is easily satisfied near threshold in switching samples: the CDW conductivity $\sigma_{\mathrm{CDW}}(I)$ is always less than or of the order of the normal conductivity σ_N, while $\sigma'_{\mathrm{CDW}}(I)$ may be arbitrarily large [if the sample shows switching, $\sigma'_{\mathrm{CDW}}(I)$ is infinite at threshold].

The steep nonlinearity which gives rise to NDR can be explained within the context of the phase-slip model of switching. The gradual depinning of nonswitching samples is usually described as a spatially homogeneous process: in pure and undamaged samples the CDW current is uniform throughout the crystal. Above the switching onset temperature, the ultrastrong-pinning centers are ineffective in causing phase slippage and switching samples behave like nonswitching samples. Well below the switching onset temperature, CDW depinning is characterized by bulk discontinuities in CDW current.[5] As dc bias is increased above a critical field, a longitudinal section of the crystal abruptly switches from the static state to a state in which the CDW is sliding with its maximum conductivity (in the high-field limit).[2] A phase-slip center only a few micrometers wide may separate the sliding section from a section of the crystal in which the CDW is pinned.[5] NDR occurs at temperatures intermediate between the switching and nonswitching regimes in a CDW crystal. We assume that small sections of the CDW behave similarly in the NDR temperature regime and in the switching temperature regime: a section either is static, or it slides with its high-field conductivity. Given this two-state assumption, it is possible to apply a current which is sufficient to depin only a fraction of the CDW. The observation of NDR indicates that, near threshold, the fraction of the CDW which is depinned is a continuous but rapidly increasing function of applied current.[28]

The rate at which the depinned fraction changes with applied current appears to be a strong function of temperature. At the relatively high temperatures at which NDR is observed, the average fraction of the CDW which is depinned changes continuously over a small range of dc bias. At the lower temperatures at which switching is observed, the depinned fraction changes abruptly. The temperature dependence of the depinning rate may be related to the temperature dependence of the coupling between the domains associated with ultrastrong-pinning centers.

The two-fluid model with a spatially inhomogeneous current distribution leads naturally to a picture of the observed instabilities. The total current is divided between a component carried by the normal electrons and a component carried by the CDW. Thus a given value of the total applied current in the NDR region does not uniquely determine the magnitude of the CDW current. In principle, for a given total current, current may shift between the normal electrons and the CDW. Such a shift causes a change in voltage across the CDW crystal. If such shifts occur erratically, noise will result. The picture of an inhomogeneous current distribution suggests a related mechanism for noise. A given value of the CDW current does not uniquely determine the spatial distribution of CDW current. For a given CDW current, the spatial distribution could shift within the crystal, causing some noise. Thus the instabilities observed in the NDR region are naturally attributed to the system hopping between distinct accessible states which have different magnitudes and spatial distributions of CDW current.

It has been shown that even the case of a system hopping between two states can lead to intermittency. Ben-Jacob *et al.*[29] have considered a Josephson junction biased to an unstable region between two stable regions where $d\theta/dt = y_1(t)$ or $d\theta/dt = y_2(t)$, where θ is the phase difference across the junction. The system may hop back and forth between states $y_1(t)$ and $y_2(t)$. In this simulation, apparently random hopping between the states leads to intermittent behavior, with a power spectrum strikingly similar to Figs. 1 and 2. A related study of bistable systems by Arecchi and Lisi[30] again finds dramatic increases in the low-frequency noise level, consistent with a $1/f$ power law. Our simultaneous observation of $1/f$ noise and intermittency suggests two different time scales for hopping in this system. The $1/f$ noise of Fig. 1 appears to be dictated by a relatively high frequency, possibly the intrinsic narrow-band-noise frequency. The intermittent behavior displayed in Fig. 2 suggests a longer time scale, of the order of 10^{-2} s. This time scale is likely related to the avalanche depinning process (see next section, ac switching noise). We conclude that NDR, large-amplitude $1/f$ noise, and intermittency may all be explained as arising from a phase-slip mechanism in which hopping occurs between many marginally stable spatial distributions of CDW current.[31]

B. ac+dc electric fields

1. ac switching noise

ac switching noise occurs when a sample is driven through the switch in the dc I-V curve at frequencies less than 1 MHz. These frequencies are low on the scale of typical narrow-band-noise frequencies (1–100 MHz), and on the scale of the crossover frequency in the ac conductivity (50 MHz). It is thus reasonable to model ac switching noise in the dc limit, ignoring dynamical effects such as entrainment or motion-dependent inertia. In the dc limit, there are two possible contributions to an increase in the broadband noise level when the sample is repeatedly driven through the switch in the I-V curve. If the sample is repeatedly depinned by a sinusoidal voltage, the power spectrum of the CDW current must include a broadband component due to the ordinary broadband noise associated with sliding CDW conduction. However, the ac switching noise of Fig. 4 is as much as 10 dB larger than the broadband noise associated with sliding CDW conduction. We propose that ac switching noise arises because the switching process itself is unpredictable.

Consider the current through a switching sample driven by a sinusoidal voltage. If the switch occurs instantaneously at exactly the same voltage for each cycle of the sinusoidal drive, then (ignoring broadband noise associated with sliding CDW conduction) the CDW current will be a perfectly periodic function of time. Only harmonics will appear in the power spectrum of the CDW current. However, if the switch occurs at a slightly different voltage for each cycle of the ac drive, or if the switch itself takes finite time to occur and is irregular, then the CDW current will not be a perfectly periodic function of time. The power spectrum of the CDW current will contain harmonics plus a broadband component. Thus the observation of ac switching noise supports the notion that switching is an unpredictable process.

The conclusion that switching is unpredictable is consistent with previous observations of Zettl and Grüner.[32] Current pulses with $I > I_C$ were applied to a switching sample. The CDW remained pinned for a time τ_{wait} after the beginning of the pulse and then depinned in a shorter time τ_{switch}. The waiting time was a random variable, distributed about its mean with a Lorentzian probability distribution. The mean τ_{wait} and the width of the distribution were found to decrease as the height of the pulse I above threshold increased. For pulse height $I = 1.01 I_C$, the average τ_{wait} was 100 μs. The switching time τ_{switch} was of the order of 1 μs.

For a switch to occur, a large fraction of the CDW must depin. This means that the domains associated with many ultrastrong-pinning centers must begin to slide at nearly the same time. An appealing picture of the onset of CDW conduction in a switching sample is that, when a critical electric field is exceeded, an avalanche of the ultrastrongly pinned domains occurs. The results of Zettl and Grüner have been modeled by Joos and Murray[33] as arising from such an avalanchelike process. The CDW is treated as a two-dimensional ribbon of identical domains (the physical origins of the domains and their couplings are not specified in this model). When an electric field exceeding threshold is applied to the crystal, each domain is assigned a probability per unit time of depinning. Once a single domain is depinned, it can trigger depinning of neighboring domains, thus setting off a "depinning wave" or avalanche. The model reproduces the waiting and switching times reported by Zettl and Grüner.[32] It is likely that the Joos-Murray model sinusoidally driven through threshold at frequencies less than $1/\tau_{\text{switch}}$ will result in power spectra similar to those for ac switching noise (a broadband component plus spikes at the drive frequency and its harmonics).

In attributing ac switching noise to a repeated avalanche process, we are invoking a many-degree-of-freedom explanation. An avalanche takes a finite amount of time to occur, as observed in switching CDW's by Zettl and Grüner. When a switching CDW is driven at frequencies greater than $1/\tau_{\text{switch}}$ (≈ 1 MHz), the avalanche will not have time to occur. A qualitatively different regime of switching CDW dynamics ensues, and is described in the next section.

2. *Mode locking*

It is crucial to include many degrees of freedom in order to understand most aspects of the dynamics of nonswitching samples.[14,15,34,35] In switching samples, many-degree-of-freedom pictures have been invoked to explain depinning, the instabilities associated with negative differential resistance, and ac switching noise. Thus it is surprising that the simplest route to chaos, the period-doubling route, occurs in switching CDW's. This route to chaos occurs in systems with a small number of active degrees of freedom. Evidently, the many-body dynamics of switching CDW's "collapses" during mode locking to a state in which only a few degrees of freedom are important. This collapse is similar to the freeze out of fluctuations observed during mode locking in nonswitching CDW's.[11] Thus, even though the dynamics of the mode-locked states in switching CDW's are more complicated than those of nonswitching CDW's, in both cases the dynamics are characterized by few degrees of freedom.

Given the low-dimensional dynamics of the mode-locked switching CDW system, it is appropriate to analyze our results mathematically in terms of low-dimensional maps and differential equations. In Sec. IV B 2 a mode locking in switching CDW's is examined in light of dynamical systems theory, and in Sec. IV B 2 b the physical mechanisms for mode locking in switching CDW's are explored. In (i) of Sec. IV B 2 a the structure of mode locking in switching CDW's is shown to be consistent with the simplest mathematical realization of a mode-locking system, the two-parameter sine circle map. For parameters appropriate to our experiments, the sine circle map predicts a period-doubling route to chaos which may be modeled by the even simpler one-parameter logistic map. In (ii) of Sec. IV B 2 a, the period-doubling route to chaos is compared to the period-doubling cascade in the presence of noise studied by Huberman and Crutchfield.[20] In (iii) of Sec. IV B 2 a, the instabilities of Figs. 8–10 are compared with predictions of Wiesenfeld[21,22] for noisy precursors of codimension-1 bifurcations.

a. Dynamical systems theory analysis. Here we examine mode locking in switching CDW's in light of dynamical systems theory.

(i) The sine circle map and the structure of mode locking. The sine circle map is a discrete mapping that has been studied extensively as a paradigm of natural systems with two competing periodicities.[18,19,36–38] Natural systems evolve in continuous time. However, all the information contained in continuous-time orbits is superfluous to an understanding of many aspects of the dynamics. Consider a periodically driven system like the (ac+dc) driven damped pendulum:[36]

$$\beta\ddot{\theta} + \dot{\theta} + \sin\theta = f_{\text{dc}} + f_{\text{ac}} \sin(\omega t) \; . \tag{6}$$

The equation is written in dimensionless form. θ is the phase of the pendulum, β is a parameter quantifying the inertia of the pendulum, f_{dc} and f_{ac} are, respectively, the dc and ac torque on the pendulum, and ω is the dimen-

sionless frequency of the ac torque. To determine the time-average phase velocity $d\theta/dt$ or the frequency of the pendulum's orbit relative to the frequency of the ac drive, it is necessary to sample the phase only once each cycle of the ac drive at $\theta_n=\theta\ (t=nT)$, where n is an integer and $T=2\pi/\omega$. It has been shown for certain parameter values that Eq. (6) may be modeled by a one-dimensional mapping of the circle (θ) onto itself.[36] The most studied member of this class of mappings is the sine circle map

$$\theta_{n+1}=\theta_n+\Omega+\frac{K}{2\pi}\sin(2\pi\theta_n)\ . \tag{7}$$

The solutions to Eq. (7) have a rich structure which has been investigated in detail by many authors.[18,19,36–38] Particular attention has been devoted to the universal scaling behavior of high-order mode-locked states near the quasiperiodic transition to chaos at $K=1$. We find that, for switching CDW's Eq. (7) has predictive power for even the low-order 0:1, 1:2, and 1:1 mode-locked states.

The structure of mode locking predicted by the circle map for the 0:1, 1:1, and 1:2 mode-locked steps is shown in Fig. 16 for $0<K<3.5$. Since θ is a mod 1 variable, the structure of mode locking is perfectly periodic in Ω, repeating itself with a periodicity 1. A detailed calculation of the structure of mode locking for $0<K<1.5$ has been performed.[37] We have added a calculation of the boundaries of the 0:1, 1:2, and 1:1 mode-locked regions for values of K up to 3.5. The boundaries of the 0:1 and 1:1 steps were determined by a simple linear stability analysis. The boundaries of the 1:2 step were calculated by iterating the circle map on a computer in the neighborhood of the boundary until the 1:2 behavior lost stability to an unlocked state.

For $K<1$, the sine circle map is a monotonically increasing function of θ. The fraction of the Ω axis occupied by mode-locked regions is a small but increasing function of K for $K<1$. When the solution is inside the 0:1 or 1:1 region, θ is at a period-1 fixed point and returns to the same value each iteration of the map. The winding number $W=\lim(\theta_N-\theta_0)/N$ is 0 (mod 1), independent of Ω. If the solution is in the 1:2 region, the winding number is $\frac{1}{2}$ independent of Ω, and θ is at a period-2 fixed point. In between the 0:1 and 1:1 steps the system alternates between higher-order mode-locked states and unlocked (quasiperiodic) states.

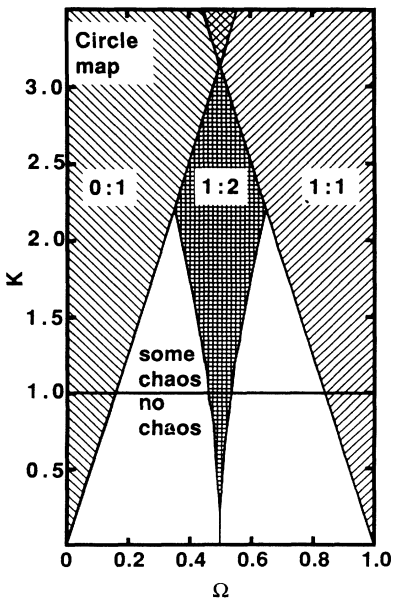

FIG. 16. 0:1, 1:2, and 1:1 mode-locked regions for the sine circle map (after Refs. 18, 19, 35, and 40). Period doubling and chaos are observed only above the solid line.

At $K=1$, the sine circle map develops an inflection point and the power spectrum develops broadband noise. This is the quasiperiodic transition to chaos, which is distinct from the period-doubling route to chaos we have observed. At $K=1$, it has been shown for the sine circle map that the space between mode-locked steps is a fractal with dimension 0.87.[18] This prediction has been verified in several physical systems.[39]

Above $K=1$, the circle map has a local maximum, and the possible states of the system are different.[37,38] At the edges of the (n:1,n:2) regions shown in Fig. 16, the solutions are mode locked as for $K<1$, with $W=(0,\frac{1}{2})$ and periodicity (1,2). As Ω is swept toward the center of the mode-locked regions, the solutions maintain their winding number but undergo period-doubling instabilities.[19] For sufficiently high K, the solutions near the centers of the mode-locked regions become unlocked and chaotic. The first period-doubled states occur inside the n:1 locked regions for $K>2$,[19] and at lower values of K for higher-order mode-locked states. For $K>\pi$, the 0:1 and 1:1 steps begin to overlap. As Ω is swept, the system jumps hysteretically from one step to the next. For K near π, as Ω is swept from the edge of a step towards the middle, a period-doubling route to chaos is observed.[40] This is consistent with experiment (see Fig. 7).

It is not straightforward to make a one-to-one correspondence between the parameters of our experiment and the parameters of the circle map. The winding number W is defined as the large-N limit of $(\theta_N-\theta_0)/N$. W is proportional to the average phase velocity of the pendulum, or in our experiment to the dc velocity of the CDW. In the absence of nonlinearity ($K=0$), $W=\Omega$. In the high-dc-field limit, V_{dc} is proportional to the CDW velocity. Since depinned switching CDW's are in the high-field limit,[2] it is reasonable to make a correspondence between Ω and V_{dc} over small ranges of dc bias. The strength of the nonlinearity K is most closely related to the experimental parameter V_{rf}. However, changing V_{rf} changes both the strength of the nonlinearity and the threshold for depinning a CDW. Thus changing V_{rf} in an experiment corresponds to changing both Ω and K in the circle map. In our comparison with the circle map, we assume that, for fixed V_{rf}, changing the dc bias between the zeroth and first mode-locked steps corresponds to changing Ω at constant K in the circle map.

Figure 17 shows the structure of mode locking for sample 2 at $T=19$ K driven by a 30-MHz rf field. The regions of 0:1 (pinned), 1:2, and 1:1 (mode locking) are plotted in the V_{dc}-V_{rf} plane.[41] At the lowest values of V_{rf} (top of this figure), there is a hysteretic transition between

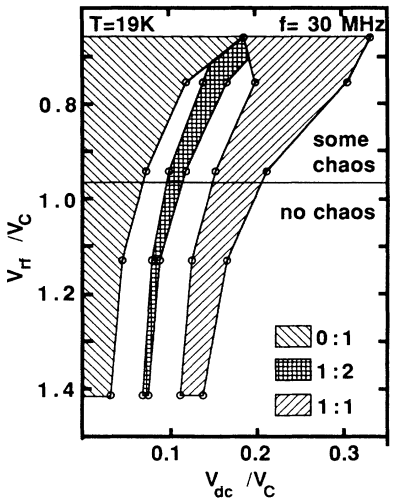

FIG. 17. 0:1, 1:1, and 1:2 mode-locked regions of sample 2 for a temperature well below the switching transition temperature. Period doubling and chaos are observed only above the solid line.

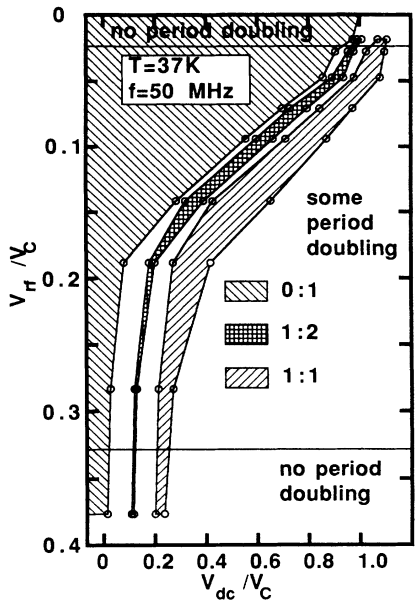

FIG. 18. 0:1, 1:2, and 1:1 mode-locked regions of sample 2 for temperature just above the switching temperature. Period doubling is observed only between the solid lines.

the 0:1 and 1:1 steps, and the 1:2 step is eclipsed. There is no space between the 0:1 and 1:1 steps. The period-doubling route to chaos is most strongly developed in this region of most hysteretic mode locking. For higher values of V_{rf} (lower in the figure) the 1:2 step emerges and a smaller fraction of parameter space is occupied by the mode-locked regions shown. Period-doubling instabilities persist, but the period-doubling cascade is not so fully developed as in the highly hysteretic region. Below the critical line drawn in this figure, the period doubling and other instabilities are no longer observed, and the 1:2 mode-locked region takes up a smaller and smaller fraction of the space between the 0:1 and 1:1 mode-locked regions.

Figure 18 shows the 0:1, 1:1, and 1:2 mode-locked steps (also for sample 2) for $f=50$ MHz and $T=37$ K, just above the switching onset temperature. For these parameters, period-2, period-4, and virtual Hopf behavior were observed, but fully developed chaos was not observed. Unlike in the low-temperature case, the 1:2 mode-locked step is always visible for this set of parameters. For low values of V_{rf}, no period-doubling instabilities are observed and the 1:2 step occupies a relatively small fraction of the space between the 0:1 and 1:1 steps. As V_{rf} is increased, the fraction first increases and then decreases. Period-doubling instabilities are observed in the intermediate range of V_{rf}. For the highest values of V_{rf}, the fraction occupied by the 1:2 step shrinks to a very small value and no period-doubling instabilities are observed.

Figures 17 and 18 demonstrate that the fraction of parameter space which is mode locked is positively correlated with the presence of dynamical instabilities. This behavior is consistent with Fig. 16, calculated from the sine circle map. However, Figs. 17 and 18 show a surprising correspondence between the parameter K in the circle map and the experimental parameter V_{rf}. At $T=19$ K, V_{rf} is negatively correlated with K: small (large) values of V_{rf} correspond to large (small) values of K. At $T=37$ K, K appears to first increase and then decrease as V_{rf} is monotonically increased. The dependence of the strength of the nonlinearity on V_{rf} will be discussed in Sec. IV B 2 b.

The period-doubling route to chaos and the structure of mode locking are both nearly periodic in dc bias over a certain range of dc bias. For instance, the 1:1, 3:2, and 2:1 mode-locked regions could have been plotted in Figs. 16–18 instead of the 0:1, 1:2, and 1:1 regions. The dependence of the widths of the mode-locked regions on V_{rf} is similar. The major difference is that the 1:1 region is narrower than the 0:1 region.

The circle map's best-known prediction[18] is that the fractal dimension of the space between mode-locked steps is 0.87 at the critical line $K=1$. The critical line is usually identified in physical systems by a sudden onset of broadband noise signaling the quasiperiodic transition to chaos. An attempt was made by Brown *et al.* to verify this prediction in nonswitching CDW's, but the critical line was not located.[10] Subsequently, the fractal dimension of the space between mode-locked steps in nonswitching CDW's has been measured for various rf amplitudes, and it was found that the fractal dimension was less than 0.87 for all values of the applied rf amplitude.[42] Thus it appears that, in the language of the circle map, mode locking in nonswitching CDW's is always subcritical (described by the circle map with $K<1$).[43]

The observation of period doubling in mode-locked switching CDW's indicates that mode locking in this system can be supercritical (period doubling occurs in the sine circle map for $K>1$). Thus it is possible to test some scaling predictions of the circle map. The critical lines in Figs. 17 and 18 separate regions in which period doubling is and is not observed in a switching CDW sam-

ple. The "dimension" of the unlocked space along these lines should be a lower bound[44] to the dimension predicted by the circle map at the quasiperiodic transition to chaos. We find[44] $d=0.85\pm0.05$ at the lower critical lines in Figs. 17 and 18. This lower bound on d is in agreement with the predictions of the circle map.

The structure of mode locking in switching CDW's is seen to be consistent with the predictions of the circle map in nontrivial ways. (1) The presence of dynamical instabilities is correlated with the width of mode-locked steps. (2) The structure of mode locking and the period-doubling route to chaos are periodic in dc bias. (3) The period-doubling cascade occurs as the system is pushed from the edge of mode-locked regions toward the middle. (4) The dimension of the space between mode-locked steps at the critical line is within experimental error of the prediction of the circle map.

(ii) Period-doubling route to chaos. The circle map has a quadratic local maximum for $K>1$. The presence of the local maximum leads to the period-doubling route to chaos, which may be described in terms of an even simpler discrete map, the one-parameter logistic map[17,45]

$$x_{n+1}=bx_n(1-x_n)\,, \tag{8}$$

where x_n is between 0 and 1 and b is between 0 and 4. As the bifurcation parameter b is increased from 0, the steady-state orbits undergo an infinite sequence of period-doubling bifurcations which accumulate geometrically at some critical parameter b_c. For $b>b_c$, the orbits are chaotic and fall in attractors with 2^m bands. As b is increased beyond b_c, these bands merge pairwise until there is only a single chaotic band. Hence there is an apparent symmetry about $b=b_c$: for $b<b_c$, the orbits are periodic with period 2^n. For $b>b_c$, the orbits are chaotic but they lie in attractors with 2^m bands and hence their power spectra look like noisy versions of 2^m periodic orbits. Huberman and Crutchfield[20] studied Eq. (9) in the presence of external noise. They showed that for a given noise level, the period-doubling cascade is truncated at some 2^m periodic orbit and the system goes into a 2^m-band attractor. All the states with period greater than 2^m and all the attractors with more than 2^m bands are washed out by the noise. The absence of high-order periodic orbits in the presence of noise has been called the "bifurcation gap."

The bifurcation gap is evident in the sequence of power spectra in Fig. 7. The period-doubling sequence is truncated at period 4. The spectrum in (iii) of Fig. 7(a) has significant noisy flanks on the sides of the period-4 subharmonics, indicating that this spectrum is between period 4 and a 4-band attractor. (iv) of Fig. 7(a), with its noise peak centered around $f/2$, is the spectrum of a two-band attractor. This sequence of spectra is a period-doubling route to chaos with all of the states between the period-4 orbit and the four-band attractor removed.

(iii) Noisy precursors. The observation of the bifurcation gap dramatizes the importance of taking into account the effects of noise in explaining our experimental results. An elegant theory of the effect of noise on codimension-1 bifurcations[46] of dynamical systems has been developed by Wiesenfeld.[21] The theory is based on the fact that a dynamical system that is near a bifurcation is almost unstable and hence is more susceptible to noise than one that is far from a bifurcation. Thus power spectra of dynamical systems near codimension-1 bifurcations exhibit bumps near the frequency at which an instability is about to occur. For instance, when a system driven at frequency f is near a period-doubling bifurcation, the theory of noisy precursors predicts that a broad bump at $f/2$ will appear before one actually observes the sharp peak at $f/2$ that signifies that the period-doubling bifurcation is complete. Another type of codimension-1 bifurcation of a periodic orbit is a Hopf bifurcation. In a Hopf bifurcation, a periodic orbit whose power spectrum has only a single frequency and its harmonics becomes unstable to a quasiperiodic orbit in which two incommensurate frequencies appear.

The noisy-precursor phenomenon most closely related to our observations is the virtual Hopf phenomenon.[22] The sequence of power spectra characteristic of this phenomenon is shown in Fig. 19. In the top trace of Fig. 19, the power spectra show bumps symmetrically located

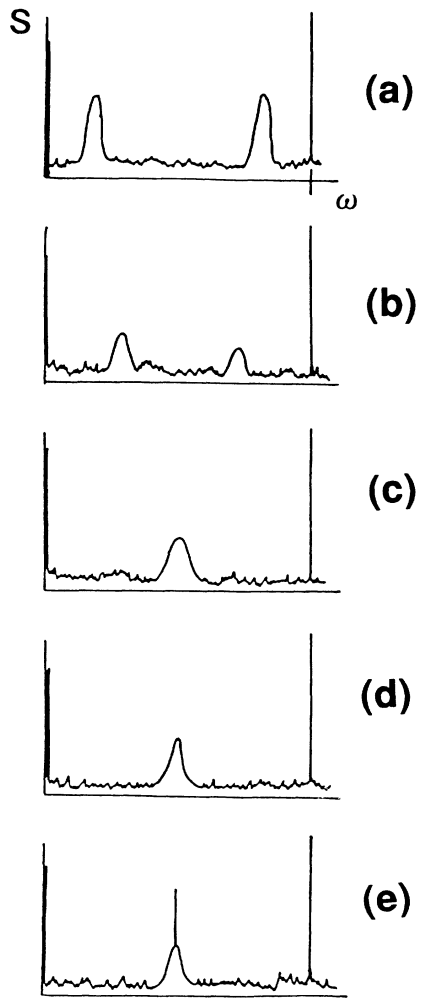

FIG. 19. Sequence of power spectra characteristic of the virtual Hopf phenomenon (reprinted from Ref. 22).

about half the driving frequency. These are the precursors to a Hopf bifurcation. However, as the bifurcation parameter is tuned, the bumps move towards $f/2$ and the spectra evolve into the precursors for a period-doubling instability. In the third trace of Fig. 19, the system has undergone a period-doubling bifurcation. The height and width of the noisy precursor peaks are related to the rate at which the system relaxes to a limit cycle after it has been kicked off the limit cycle by a perturbation. The width of the noisy-precursor peak is a measure of the longest relaxation time of the system. It has been argued that this phenomenon should be common in dynamical systems exhibiting a period-doubling instability.

The sequence of power spectra presented in Fig. 8 resembles very closely the sequence characteristic of the virtual Hopf phenomenon. Figure 9 is not identical to the virtual Hopf phenomenon, but the appearance and disappearance of broad bumps in the power spectrum is strongly suggestive of a noisy-precursor explanation. From the 1-MHz width of the broad bumps in both Figs. 8 and 9, we extract a relaxation time of the order of 1 μs. The spectra in Fig. 10 may also have a noisy-precursor explanation.

An alternate explanation of the spectra in Fig. 8 is possible. The spectra in this figure look very much like spectra observed during mode locking of ordinary nonswitching samples.[13] The broad bumps that travel through the spectrum could be interpreted as narrow-band noise peaks which become mode locked on subharmonic steps when the peaks sharpen into period 3 and period 2. This explanation is problematic because the appearance of a strong peak at $f/2$ did not necessarily coincide with the observation of an n:2 step in the differential resistance. This matter requires further investigation. There is no easy explanation for the spectra in Fig. 9 as arising from narrow-band noise in conventional mode locking.

b. Physical mechanisms of mode locking and period doubling. Section IV B 2 a classified certain aspects of mode locking in switching CDW's as manifestations of behavior common in simple nonlinear dynamical systems. This section examines mode locking in ac-dc driven switching CDW's in terms of the underlying physical processes. Period doubling and chaos in switching CDW's are explained as the frustrated response of a strongly entrained system with a motion-dependent inertia.[3,4] Period doubling and chaos occur over a limited range of driving frequencies, driving amplitudes, and dc biases. These boundaries for nonlinear behavior are qualitatively explained and it is suggested that switching CDW's depolarize on a time of the order of 1 μs. The physical relevance of the circle-map nonlinearity parameter K is discussed.

Inertia does not appear to play any role in nonswitching CDW transport.[1] In contrast, mode locking in switching CDW's has many characteristics of an inertial, underdamped response.[6] The symptoms of nonnegligible inertia are hysteresis in the dc I-V curve, and the inductive ac conductivity observed in switching CDW's biased past threshold.[3,6] The simplest differential equation which incorporates inertia and exhibits mode locking is the much-studied pendulum equation [Eq. (6)]. The solutions to this equation share many of the features of the experimentally observed behavior of mode-locked switching CDW's. For $\beta > 1$ (underdamped), the solutions to the pendulum equation exhibit hysteretic Shapiro steps, and a period-doubling route to chaos is observed on some of these Shapiro steps.[47–49] We conclude that some pseudoinertia plays a significant role in switching CDW transport.

The underdamped pendulum equation does not agree in detail with the behavior of switching CDW's.[3,4,6] The ac conductivity of a switching CDW with no applied dc field appears overdamped. This is contrary to the prediction of Eq. (6), and indicates that the pseudoinertia is only effective when the CDW is in motion.[3,4] Equation (6) predicts a chaotic response[47] only for drive frequencies $\beta^{-1} < \omega < \beta^{-1/2}$. This is a much narrower range than observed in switching CDW's. Finally, the period-doubling route to chaos in Eq. (6) is not periodic in dc bias as it is in CDW's.[47] The period-doubling route may occur on one step, then skip the next step. In fact, as dc bias is increased in Eq. (6), mode-locked steps are not necessarily visited in order of increasing winding number.[47] In switching CDW's, these steps are always visited in order of increasing winding number (e.g., the CDW current increases monotonically with dc bias).

The phase-slip process gives rise to a motion-dependent inertia which can qualitatively account for the chaotic response of a switching CDW.[3,4] The phase-slip process requires a macroscopic polarization of the CDW prior to the collapse of the CDW amplitude. After the amplitude collapse, it takes a finite time τ for the CDW to depolarize and slide. This lag in the response is equivalent to inertia (in inertial systems, the response lags the force). When the phase-slip process is entrained at a frequency of order $1/\tau$, the CDW's tendency to follow the external forcing may compete with its requirement to "remember" its previous polarization state. This competition leads to a frustrated subharmonic or chaotic response. Period doubling occurs both just above and below the switching onset temperature. The period doubling observed just above the switching onset temperature can also be attributed to the polarization-induced inertia, because at these temperatures significant polarization may occur without a hysteretic switch.

The longest depolarization time provides a natural lower bound on the rf frequency required to produce a frustrated response. (There may in principle be many depolarization times in a given sample, and the distribution of these times may depend on driving conditions.) Period doubling and chaos occurred in our measurements on sample 2 only for driving frequencies greater than 1 MHz, suggesting that the longest depolarization time in this sample was of the order of 1 μs. Other experimental results also suggest that the longest depolarization times τ in switching samples are of the order of 1 μs. The width of a noisy precursor reflects the longest relaxation time of a system. The noisy precursors shown in Figs. 7 and 8 for sample 3 have widths of order 1/1 μs. The switching time τ_{switch} ascertained from pulsed experiments is also likely related to the depolarization time.

Measurements on a different sample by Zettl and Grüner[32] found τ_{switch} of the order of 1 μs. There are also upper bounds in parameter space for the observability of period-doubling and related instabilities. The disappearance of these frustrated responses for large rf amplitude, dc bias, or rf frequency can be attributed to a suppression of motion-dependent inertia. If the CDW is forced to move too rapidly, the polarization and depolarization which are inherent to the phase-slip process do not have time to occur. The motion-dependent inertia is suppressed. In the absence of motion-dependent inertia, the switching samples should behave like nonswitching samples. this similarity is borne out in Figs. 6 and 15. For the rf amplitudes above which period-doubling instabilities are observed, the differential conductance curves look similar to those for nonswitching CDW's. As a function of dc bias, there is a relatively small ratio of locked to unlocked space in these high rf amplitudes.

It is now possible to make a physical interpretation of the nonlinearity parameter K in the circle map. Period doubling and chaos in switching CDW's occur for large values of K (small space between mode-locked steps). However, K *decreases* as rf amplitude is increased to large values. It was argued above that motion-dependent inertia should also decrease as rf amplitude is increased. Thus it appears that K is correlated with the motion-dependent inertia of the switching CDW system.

There is a more general mathematical argument for the presence of an upper boundary on the region in which period-doubling instabilities are observed. When a nonlinear differential equation is forced sufficiently strongly, the nonlinearity becomes a mere perturbation on a linear system.[14,15] The dimensionless overdamped pendulum equation [Eq. (6) with $\beta=0$] illustrates the reduction of the effective nonlinearity of a system by strong forcing:

$$\dot{\theta}+\sin\theta=e_{\text{dc}}+e_{\text{ac}}\sin(\omega t)\ . \tag{9}$$

Consider the limits $e_{\text{dc}}\gg 1$, $e_{\text{rf}}\approx 1$, $\omega\approx 1$, $e_{\text{rf}}\gg 1$, $e_{\text{dc}}\approx 1$, $\omega\approx 1$, $e_{\text{dc}}\approx 1$, $e_{\text{rf}}\approx 1$, and $\omega\gg 1$. In the limit of large $(e_{\text{dc}},e_{\text{ac}},\omega)$, $d\theta/dt$ is of the order of $(e_{\text{dc}},e_{\text{ac}},\omega)$, while the nonlinear term $\sin\theta$ is much smaller, of order 1. For large driving parameters, the effective nonlinearity of the overdamped pendulum equation becomes small. A similar analysis for the pendulum equation with finite mass is more complicated. However, it is expected that for large driving parameters, the effective nonlinearity of the underdamped pendulum equation will also be reduced. The upper boundaries in V_{dc}, V_{rf}, and ω can be attributed to the decreased effective nonlinearity of the switching CDW system for large driving parameters. The argument also explains why the widths of Shapiro steps in nonswitching samples decreases at high values of V_{rf}.[15]

V. CONCLUSION

The dynamical instabilities observed in switching CDW's can be divided into two categories. Instabilities in the first category occur for low driving frequencies. These instabilities include the $1/f$ noise and intermittency observed for current-driven switching CDW's in a NDR region, and the ac switching noise observed for combined low-frequency dc and ac electric fields. The low-frequency instabilities are attributed to the many-degree-of-freedom dynamics of the many-phase-slip domains. The instabilities in the second category occur for high-frequency (>1 MHz) driving electric fields. The high-frequency instabilities are the period-doubling route to chaos and related instabilities. For high driving frequencies, the independent switching CDW domains are synchronized by the rf electric field, causing the many-degree-of-freedom dynamics of the switching CDW system to collapse onto a subsystem with few dynamical variables. The collapsed dynamical system undergoes the period-doubling route to chaos, which is characteristic of systems with few degrees of freedom. The one-dimensional circle map, the logistic map, and the theory of noisy precursors explain many details of the second category of instabilities. Physically, period doubling in this case may be viewed as the frustrated response of an inertial CDW which is strongly entrained by a radio-frequency electric field. The CDW inertia arises naturally from the phase-slip process.

This paper has for the first time presented and classified a rich and varied assortment of instabilities observed in switching CDW's. This paper represents the most successful application of the modern theory of nonlinear dynamical systems to the study of CDW systems. There is much room for further application of the tools of nonlinear dynamics to the study of this rich system. For instance, the theory of nonlinear dynamical systems provides a quantitative method for estimating the number of degrees of freedom involved in a chaotic process. The required procedure is to calculate the Hausdorff dimension of a chaotic attractor from a chaotic time series. This procedure is difficult to implement in switching CDW's because of the high frequencies involved. Experiments are planned to directly determine the number of degrees of freedom involved in the chaotic dynamics of switching CDW's by measuring the Hausdorff dimension of the instabilities of switching CDW's.

ACKNOWLEDGMENTS

We thank P. Bak, S. Bhattacharya, P. B. Bryant, S. Coppersmith, M. F. Hundley, M. H. Jensen, C. D. Jeffries, P. B. Littlewood, P. Parilla, S. Teitsworth, R. M. Westervelt, and K. Wiesenfeld for helpful discussions. This work was supported by National Science Foundation (NSF) Grant No. DMR-84-00041. One of us (M.S.S.) also acknowledges support from AT&T Bell Laboratories, and another (A.Z.) acknowledges support from the Alfred P. Sloan Foundation. The work of one of us (R.P.H.) was done at the University of California at Berkeley.

*Current address: Department of Physics, University of California, Santa Barbara, CA 93106.

[1]For a review of nonswitching CDW conduction, see G. Grüner and A. Zettl, Phys. Rep. **119**, 117 (1985).

[2]R. P. Hall, M. F. Hundley, and A. Zettl, this issue, Phys. Rev. B **38**, 13 002 (1988).

[3]R. P. Hall and A. Zettl, preceding paper, Phys. Rev. B **38**, 13 019 (1988).

[4]M. Inui, R. P. Hall, S. Doniach, and A. Zettl, following paper, Phys. Rev. B **38**, 13 047 (1988).

[5]R. P. Hall, M. F. Hundley, and A. Zettl, Phys. Rev. Lett. **56**, 2399 (1986).

[6]R. P. Hall and A. Zettl, Solid State Commun. **50**, 813 (1984).

[7]R. P. Hall, M. S. Sherwin, and A. Zettl, Phys. Rev. Lett. **52**, 2293 (1984).

[8]P. Monceau, J. Richard, and M. Renard, Phys. Rev. Lett. **45**, 43 (1980).

[9]A. Zettl and G. Grüner, Solid State Commun. **46**, 501 (1983).

[10]S. E. Brown, G. Mozurkewich, and G. Grüner, Phys. Rev. Lett. **54**, 2272 (1984).

[11]M. S. Sherwin and A. Zettl, Phys. Rev. B **32**, 5536 (1985).

[12]R. P. Hall and A. Zettl, Phys. Rev. B **30**, 2279 (1984).

[13]S. Bhattacharya, J. P. Stokes, M. J. Higgins, and R. A. Klemm, Phys. Rev. Lett. **59**, 1849 (1987).

[14]L. Sneddon, M. C. Cross, and D. S. Fisher, Phys. Rev. Lett. **49**, 292 (1982).

[15]S. N. Coppersmith and P. B. Littlewood, Phys. Rev. Lett. **57**, 1927 (1986).

[16]R. P. Hall, M. S. Sherwin, and A. Zettl, Phys. Rev. B **29**, 7076 (1984).

[17]See, for example, J. M. T. Thompson and H. B. Stewart, *Nonlinear Dynamics and Chaos* (Wiley, Somerset, NJ, 1986).

[18]M. H. Jensen, P. Bak, and T. Bohr, Phys. Rev. Lett. **50**, 1637 (1983).

[19]L. Glass and R. Perez, Phys. Rev. Lett. **48**, 1772 (1983).

[20]J. P. Crutchfield and B. A. Huberman, Phys. Lett. A **77**, 407 (1980).

[21]K. Wiesenfeld, J. Stat. Phys. **38**, 1071 (1985).

[22]K. Wiesenfeld, Phys. Rev. A **32**, 1744 (1985).

[23]R. P. Hall and A. Zettl, Solid State Commun. **50**, 813 (1984).

[24]R. P. Hall, M. F. Hundley, and A. Zettl, Synth. Met. **19**, 813 (1987).

[25]J. P. Stokes, S. Bhattacharya, and A. N. Bloch, Phys. Rev. B **34**, 8944 (1986).

[26]A. Zettl and G. Grüner, Phys. Rev. B **29**, 755 (1984).

[27]R. P. Hall, M. F. Hundley, and A. Zettl, Physica **143B**, 152 (1986).

[28]We cannot rule out the possibility that the current distribution is spatially homogeneous in the NDR region. However, the picture of an inhomogeneous distribution is consistent with observations of inhomogeneous current distributions and switching.

[29]E. Ben-Jacob, I. Goldhirsch, Y. Imry, and S. Fishman, Phys. Rev. Lett. **49**, 1599 (1982).

[30]F. T. Arecchi and F. Lisi, Phys. Rev. Lett. **49**, 94 (1982).

[31]There is much literature on negative differential conductivity (NDC) in semiconductors. (For a review, see Eckerhardt Schöll, Adv. Solid State Phys. **26**, 309 (1986), and A. F. Volkov and Sh. M. Kogan, Usp. Fiz. Nauk. **96**, 633 (1968) [Sov. Phys.—Usp. **11**, 881 (1969)].) Two types of NDC are observable in semiconductors. In so-called SNDC, the current-voltage curve (CVC) is "S" shaped and the current is a multiple-valued function of the voltage. In NNDC, the CVC is "N" shaped, and the current is a single-valued but non-monotonic function of the electric field. The NDC we have observed in switching CDW's is SNDC. In semiconductors, current distributions in static states of NDC are spatially homogeneous. These homogeneous static states are unstable to dynamic states with inhomogeneous current distributions. The most famous such instability in semiconductors is the Gunn effect, in which a static NNDC state becomes unstable to a state with traveling domains which emit microwave frequency oscillations. The case of CDW's is quite different. In a CDW, the *static* NDR state appears to be spatially inhomogeneous.

[32]A. Zettl and G. Grüner, Phys. Rev. B **26**, 2298 (1982).

[33]B. Joos and D. Murray, Phys. Rev. B **29**, 1094 (1984).

[34]R. M. Fleming and L. F. Schneemeyer, Phys. Rev. B **33**, 2930 (1986); S. E. Brown, G. Grüner, and L. Mihaly, Solid State Commun. **57**, 165 (1986).

[35]C. Tang, K. Wiesenfeld, P. Bak, S. Coppersmith, and P. B. Littlewood, Phys. Rev. Lett. **58**, 1161 (1987).

[36]T. Bohr, P. Bak, and M. H. Jensen, Phys. Rev. A **30**, 1970 (1984).

[37]M. H. Jensen, P. Bak, and T. Bohr, Phys. Rev. A **30**, 1960 (1984); P. Bak, Phys. Today **39**, 38 (1986).

[38]T. Bohr and G. Gunaratne, Phys. Lett. A **113**, 55 (1985).

[39]J. Stavans, F. Heslot, and A. Libchaber, Phys. Rev. Lett. **55**, 596 (1985); E. G. Gwinn and R. M. Westervelt, *ibid.* **59**, 157 (1987); S. Martin and W. Martienssen, *ibid.* **56**, 1522 (1986).

[40]M. S. Sherwin (unpublished).

[41]We have defined the boundary of a mode-locked region as the point at which the differential conductance begins to drop from the high (unlocked) value. At high rf amplitudes, where there were two sets of interference peaks corresponding to two domains with different narrow-band noise frequencies, only the mode-locked regions corresponding to the lower-velocity narrow-band-noise domain are recorded.

[42]A. Zettl, Physica D **23**, 155 (1986).

[43]Coppersmith and Littlewood have argued that subharmonic mode locking in nonswitching CDW's is intrinsically a many-degree-of-freedom effect, and hence that the predictions of the circle map are not relevant to mode locking in nonswitching CDW's. We do not address here the relevance of the circle map to mode locking in nonswitching CDW's. If we *assume* that a circle-map description is valid, then mode locking in nonswitching CDW's appears subcritical (based on the scaling of the space between mode-locked steps) and is consistent with the absence of period doubling or chaos.

[44]We have calculated the dimension d from the space between the 0:1, 1:2, and 1:1 mode-locked steps using an algorithm proposed by P. Cvitanović, M. H. Jensen, L. P. Kadanoff, and I. Procaccia [Phys. Rev. Lett. **55**, 343 (1985)]. They have shown empirically that the fractal dimension may be calculated to within 1% accuracy by considering only the space between three relatively high-order mode-locked steps that are neighbors in a branch of a Farey tree: steps with winding number p/q, p'/q', and $(p+p')/(q+q')$. The dimension is given by $(s_1/S)^d+(s_2/S)^d=1$, where S is the space between steps p/q and p'/q', and s_1 and s_2 are, respectively, the space between p/q and $(p+p')/(q+q')$ and between $(p+p')/(q+q')$ and p'/q'. We tested the accuracy of this equation for low-order mode-locked states. A value $d=0.875$ was calculated using this equation and the space between the 0:1, 1:1, and 1:2 mode-locked steps predicted by the circle map at $K=1$. This is within 1% of the value $d=0.868$ calculated using scaling arguments with many high-order mode-locked steps (Ref. 18). In switching CDW's, a quasiperiodic

transition to chaos was not directly observed (perhaps it was obscured by the conduction noise associated with sliding CDW conduction). However, a line was observed (Figs. 17 and 18) which separates regions of parameter space in which period doubling is observed from regions in which it is not. The sine circle map predicts that the onset of period doubling occurs at higher K values (wider mode-locked steps) than the quasiperiodic transition to chaos. Thus the dimension of the unlocked space along the lines drawn to Figs. 17 and 18 represents a lower bound on the dimension of the complete devil's staircase which occurs in the circle map at $K=1$.

[45]R. H. May, Nature (London) **261**, 459 (1976); M. J. Feigenbaum, J. Stat. Phys. **19**, 25 (1978).

[46]Codimension-1 bifurcations are those that are achieved by changing only one parameter: saddle-node, transcritical, pitchfork, period-doubling, and Hopf bifurcations. See, for instance, J. Guckenheimer and E. Holmes, *Nonlinear Oscillations, Dynamical Systems, and Bifurcations of Vector Fields* (Springer-Verlag, New York, 1983), pp. 145–156.

[47]R. L. Kautz, Appl. Phys. Lett. **52**, 6241 (1981).

[48]D. D'Humières, M. R. Beasley, B. A. Huberman, and A. Libchaber, Phys. Rev. A **26**, 3483 (1982).

[49]A. H. MacDonald and M. Plischke, Phys. Rev. B **27**, 201 (1983).